Observation of State and Topology in DC Networks

Tuncay Altun, *Student Member, IEEE*, Ramtin Madani, *Member, IEEE*, and Ali Davoudi, *Senior Member, IEEE*

***Abstract*—This paper copes with the state estimation and topology identification problems in direct current (DC) networks. This problem is challenging due to binary decisions and nonlinear relations between sensor measurements and state variables. We introduce a non-convex nuclear norm estimator whose non-convexity is addressed by incorporating two inertia terms. In the presence of noise, penalty terms are integrated into the objective function to estimate unknown noise values. Numerical results for the modified IEEE 9-bus, 14-bus, and 30-bus systems corroborate the merits of the proposed technique. Furthermore, this technique is experimentally validated for a converter-augmented 14-bus system in a real-time hardware-in-the-loop platform.**

***Index Terms*—Convex optimization, DC network, state estimation, topology identification.**

I. Introduction

DIRECT current (DC) networks are gaining prominence with the increasing penetration of DC loads, storages, and sources, since they offer improved efficiency in conversion/distribution over alternating current (AC) networks. For static distribution topologies, estimation techniques can extract the system state to be used in network analysis, control, optimization, or diagnostic under normal, emergency, or restorative operations [1]. The most recent topology information is needed to meaningfully carry out the state estimation process; any error or misconfiguration in the assumed topology could result in inappropriate control decisions [2], [3]. Incorporating statuses of the lines, that collectively describe the overall network topology, into the state estimation process is challenging as they introduce binary variables [4], [5]. Moreover, converter-populated DC networks might employ fewer sensors due to cost, security, or privacy concerns, leading to low-observability conditions.

The state estimation process is conventionally expressed as a nonlinear least-squares problem [6]. The weighted least-squares (WLS) estimation criterion has been employed in practice to filter out Gaussian measurement noise with certain statistical properties [7], [8]. As WLS is susceptible to gross measurement errors, other gross error detection and identification methods have been proposed to perform accurate state estimation [8]–[12]. Given their non-convex problem formulation, the Gauss-Newton algorithm is sensitive to the initial points, and might converge to local minima [13]. Convex relaxation methods can either directly solve the estimation problem [14] or provide an initial guess for the Newton's method [15]. Convergence guarantees for the estimation process using convex relaxation techniques are given in [16]. With measurement redundancy, incorporating penalty terms in the formulation of the objective function can help cleansing noise and bad data [17]–[19]. These techniques, however, assume a fixed network topology.

Topology identification is either a prerequisite to the estimation process, or should be considered concurrently. The combined problem can be handled using a Gauss-Newton, e.g., generalized state estimation (GSE) [4], or convex relaxation methods [5]. Inverse power flow formulation can describe the network topology through a nodal admittance matrix [20]. These studies usually assume imperfect but highly-redundant measurement. Low-observability condition refers to the sparse sensor that results in an under-determined system. With proper placement, fewer sensors might be needed to observe the network [21], [22]. [23] finds the required minimal set of measurement so that an unobservable network can become observable. Alternative non-iterative numerical solutions are proposed in [24], [25]. However, even an observable network may temporarily become unobservable due to topological changes or failure in the communication. The sensor placement procedures, considering topology changes or communication failures, are developed in [26]–[28]. Additional sensors placement [29] or pseudo measurements from existing sensors data [30] come with an additional cost, computational burden, or estimation errors [31].

The matrix completion method, that offers a solution to an under-determined system, has been applied to distribution networks with poor sensors installation [32], [33]. While the joint state estimation and topology identification problem has been studied for AC networks [5], its solution has not yet been elaborated under low-observability conditions [31], [34]–[37]. Moreover, state estimation and topology identification of DC networks are rare in the literature [38]–[40], and have not even considered the observability conditions.

We leverage the physical properties of DC networks to develop a joint estimation and topology identification algorithm using a limited number of measurement. We formulate this as a non-convex mixed-binary problem, develop a non-convex nuclear norm estimator, and address this non-convexity by using two inertia terms. The presence of zero injection buses (i.e.,

Manuscript received July 24, 2019; revised December 11, 2019, April 1, 2020, and June 17, 2020; accepted August 4, 2020. Date of publication August 10, 2020; date of current version February 19, 2021. This work was supported by the National Science Foundation under Award ECCS-1809454. Paper no. TPWRS-01084-2019. *(Corresponding author: Ali Davoudi.)*

The authors are with the University of Texas, Arlington, TX 76019 USA (e-mail: tuncay.altun@mavs.uta.edu; ramtin.madani@uta.edu; davoudi@uta.edu).

Color versions of one or more of the figures in this article are available online at https://ieeexplore.ieee.org.

Digital Object Identifier 10.1109/TPWRS.2020.3015426

a bus with no load or converter) is used to strengthen the convex relaxation and decrease the number of required sensors. The resulting formulation does not rely on prior knowledge of unmonitored line-statuses, current, or power flow measurements that could infer topology information. The devised convex optimization framework is robustified against noise by upgrading to a penalized convex program. This formulation is in a generic form, and can be solved with various numerical solvers.

The rest of this paper has the following organization: Section II discusses the preliminaries. Section III presents the joint state estimation and topology identification problem for noiseless measurements. This non-convex problem is transformed into convex surrogate using two inertia terms and, then, extended to accommodate noisy measurements. In Section IV, the resulting state estimation and topology identification solution is verified through numerical and experimental benchmarks. Section V finalizes the paper.

II. Notations and Terminologies

A. Notations

Throughout this paper, bold uppercase ($\boldsymbol{A}$) and lowercase letters ($\boldsymbol{a}$) refer to the matrices and vectors, respectively. The symbols $\mathbf{1}_n$ and $\mathbf{0}_n$ represent $n \times 1$ vectors of ones and zeros, respectively. $\mathbf{0}_{n\times m}$ refers to a zero matrix of size $n \times m$. $\boldsymbol{I}_{n\times n}$ indicates an identity matrix of size $n \times n$. The symbol $\mathbb{R}$ defines the sets of real numbers. The entries of a matrix are presented by indices (i, j). $(\cdot)^\top$ indicates the transpose of a matrix. $|\cdot|$ refers the cardinality of a set or the absolute value of a vector/scalar. $Tr(\cdot)$ shows to the trace of a matrix. $\|\cdot\|_2$ stands for the euclidean norm of its argument vector. $\|\cdot\|_*$ represents the nuclear norm of its argument matrix. A vector composed from diagonal entries of a matrix is shown by $\mathrm{diag}\{\cdot\}$. $\boldsymbol{X} \succeq 0$ indicates a positive semi-definite matrix.

B. Terminologies

On a DC network, distribution lines are resistive and DC-DC power electronics converters interface energy resources to the distribution network as demonstrated in Fig. 1. DC network can be articulated using a directed graph, $\mathcal{H} = (\mathcal{N}, \mathcal{L})$ with $\mathcal{N}$ and $\mathcal{L}$ sets, respectively, representing buses and lines. Every bus can accommodate a DC-DC converter, a resistive load, and/or a constant power load.

Define the pair $\vec{\boldsymbol{L}}, \overleftarrow{\boldsymbol{L}} \in \{0, 1\}^{|\mathcal{L}|\times|\mathcal{N}|}$, respectively, as the *from* and *to* line incidence matrices. $\vec{\boldsymbol{L}}_{l,i} = 1$ if the line l starts at bus i. $\overleftarrow{\boldsymbol{L}}_{l,i} = 1$ implies that the line l ends at bus i. The conductance of a line $l \in \mathcal{L}$ is g_l, with $\boldsymbol{g} \in \mathbb{R}^{|\mathcal{L}|}$ as the line conductance vector. $\boldsymbol{G} \in \mathbb{R}^{|\mathcal{N}|\times|\mathcal{N}|}$ is the bus conductance matrix. $\vec{\boldsymbol{G}}$ and $\overleftarrow{\boldsymbol{G}} \in \mathbb{R}^{|\mathcal{L}|\times|\mathcal{N}|}$ are, respectively, the *from* and *to* line conductance matrices.

Let n define the number of buses, i.e., $n = |\mathcal{N}|$. $\boldsymbol{v} = [v_1, v_2, \ldots, v_n]^\top$ is the vector of voltages with $v_k \in \mathbb{R}$ as the voltage at bus $k \in \mathcal{N}$. Let $i_k \in \mathbb{R}$ refer to the current-injection at bus $k \in \mathcal{N}$, while $\boldsymbol{i} = [i_1, i_2, \ldots, i_n]^\top$ is the corresponding vector. Given a line $l \in \mathcal{L}$, there are two current signals, $\vec{i}_l \in \mathbb{R}$ and $\overleftarrow{i}_l \in \mathbb{R}$, entering the line via its $from$ and to ends, respectively.

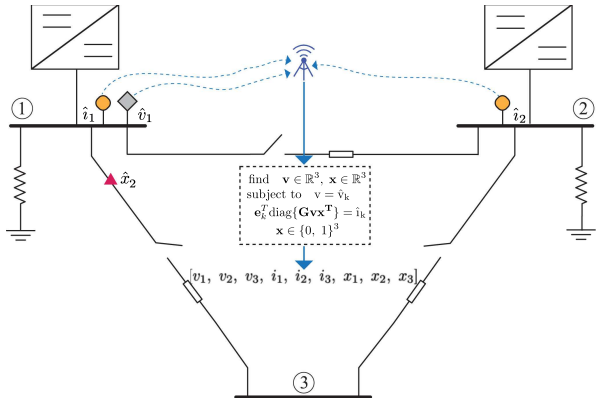

Fig. 1. Three bus DC distribution network is equipped with sensors at buses 1 and 2 and the line between buses 1-3 to collect data $(\hat{v}_1, \hat{x}_2, \hat{\imath}_1, \hat{\imath}_2)$. Optimizer jointly performs state estimation and topology identification using these limited measurements, and infers unknown voltage, v_2, v_3, and statuses of the lines, x_1, x_3.

$\vec{\boldsymbol{\imath}} = [\vec{\imath}_1, \vec{\imath}_2, \ldots, \vec{\imath}_{|\mathcal{L}|}]^\top$ and $\overleftarrow{\boldsymbol{\imath}} = [\overleftarrow{\imath}_1, \overleftarrow{\imath}_2, \ldots, \overleftarrow{\imath}_{|\mathcal{L}|}]^\top$ are the vectors of corresponding composites. We assume there is no interlinking converter in the network; hence $\vec{\boldsymbol{\imath}} = -\overleftarrow{\boldsymbol{\imath}}$. $\hat{v}_k, \hat{\imath}_k$, and $\hat{x}_l$ denote the measured voltage as well as the current-injection at bus $k \in \mathcal{N}$, and the status of line $l \in \mathcal{L}$, respectively. v_k and x_l refer to the estimated voltage at bus $k \in \mathcal{N}$, and the identified status of the line $l \in \mathcal{L}$, respectively.

III. Joint State Estimation and Topology Identification

A. Problem Formulation

We will exploit the power flow equations of a DC network to express this problem as a constrained minimization program. The available measurements are: (i) voltage values at some of the randomly-chosen buses, (ii) current-injection values at some of the randomly-chosen buses, and (iii) some of the line statuses. The Ohm's law dictates that the current flow from both sides of each line, and the current-injection at each bus, can be respectively represented as

$$\vec{\boldsymbol{\imath}} = \mathrm{diag}\{\vec{\boldsymbol{G}}\, \boldsymbol{v}\, \boldsymbol{x}^\top\}, \qquad \overleftarrow{\boldsymbol{\imath}} = -\vec{\boldsymbol{\imath}}, \tag{1}$$

$$\boldsymbol{i} = \vec{\boldsymbol{L}}^\top \vec{\boldsymbol{\imath}} + \overleftarrow{\boldsymbol{L}}^\top \overleftarrow{\boldsymbol{\imath}}. \tag{2}$$

Note that (1) and (2) hold true unless there is an interlinking converter on the line.

The state estimation and topology identification algorithm simultaneously finds the voltage vector, $\boldsymbol{v}$, and the line-status vector, $\boldsymbol{x}$, while satisfying all the measurement equations

$$\text{find} \qquad \boldsymbol{v} \in \mathbb{R}^{|\mathcal{N}|}, \boldsymbol{x} \in \mathbb{R}^{|\mathcal{L}|} \tag{3a}$$

$$\text{subject to} \qquad v_k = \hat{v}_k \qquad \forall k \in \mathcal{S}_v \tag{3b}$$

$$\boldsymbol{e}_k^\top \mathrm{diag}\{\boldsymbol{G}\boldsymbol{v}\boldsymbol{x}^\top\} = \hat{\imath}_k \qquad \forall k \in \mathcal{S}_i \tag{3c}$$

$$\boldsymbol{x}^{\mathrm{lb}} \le \boldsymbol{x} \le \boldsymbol{x}^{\mathrm{ub}} \tag{3d}$$

$$\boldsymbol{x} \in \{0, 1\}^{|\mathcal{L}|} \tag{3e}$$

where $\{\boldsymbol{e}_1,\ldots,\boldsymbol{e}_N\}$ are the basis vectors in $\mathbb{R}^n$. Here, measurement equations refer to the nonlinear relations between sensor outputs and state variables as in (3c). For $x^{\rm lb}$ and $x^{\rm ub}$, the conditional expressions can be given as

$$\begin{aligned}
&x_l{}^{\rm lb}=x_l{}^{\rm ub}=1, && \text{if line } l\in\mathcal{L} \text{ is known to be connected,}\\
&x_l{}^{\rm lb}=x_l{}^{\rm ub}=0, && \text{if line } l\in\mathcal{L} \text{ is known to be disconnected,}\\
&x_l{}^{\rm lb}=0,\quad x_l{}^{\rm ub}=1, && \text{if the status of line } l \text{ is undetermined.}
\end{aligned}$$

Here, $x_l{}^{\rm lb}$ and $x_l{}^{\rm ub}$ refer to the lower and upper bound of line statuses.

Equation (3b) enforces the voltage value to be equal to the sensor measurement if the corresponding bus is equipped with a voltage sensor (i.e., *a monitored bus*). v_k and $\hat{v}_k$ denote voltage values to be estimated and to be measured for every bus $k\in\mathcal{S}_v$, respectively. $\mathcal{S}_v$ denotes the set of voltage measurements. Equality constraint (3c) aims to find the voltage value and line status that fit the corresponding input value, $\hat{\imath}_k$, from a set of current-injection measurements, $\mathcal{S}_i$. Problem (3) is non-convex because of vector multiplication in $\boldsymbol{v}\boldsymbol{x}^\top$ and the binary variables accounting for the statuses of the lines. Next, we offer a convex reformulation alternative.

B. Convexification of the Problem Formulation

We introduce the following convex optimization problem using the auxiliary variable $\boldsymbol{A}$ accounting for $\boldsymbol{v}\boldsymbol{x}^\top$

$$\underset{\substack{\boldsymbol{A}\in\mathbb{R}^{|\mathcal{N}|\times|\mathcal{L}|}\\ \boldsymbol{v}\in\mathbb{R}^{|\mathcal{N}|}\\ \boldsymbol{x}\in\mathbb{R}^{|\mathcal{L}|}}}{\text{minimize}} \quad \|\boldsymbol{M}^{\frac{1}{2}}(\boldsymbol{A}-\boldsymbol{v}\boldsymbol{x}^\top)\boldsymbol{N}^{\frac{1}{2}}\|_*+\|\boldsymbol{v}-\boldsymbol{v}_0\|^2_{\boldsymbol{M}}+\|\boldsymbol{x}-\boldsymbol{x}_0\|^2_{\boldsymbol{N}} \tag{4a}$$

$$\text{subject to} \quad v_k=\hat{v}_k \qquad \forall k\in\mathcal{S}_v \tag{4b}$$

$$\boldsymbol{e}_k^\top \text{diag}\{\boldsymbol{G}\boldsymbol{A}\}=\hat{\imath}_k \qquad \forall k\in\mathcal{S}_i \tag{4c}$$

$$\boldsymbol{e}_k^\top\boldsymbol{A}=\hat{v}_k\boldsymbol{x}^\top \qquad \forall k\in\mathcal{S}_v \tag{4d}$$

$$\boldsymbol{A}\boldsymbol{d}_l^\top=\boldsymbol{v}\hat{x}_l \qquad \forall l\in\mathcal{S}_x \tag{4e}$$

$$\boldsymbol{x}^{\rm lb}\le\boldsymbol{x}\le\boldsymbol{x}^{\rm ub} \tag{4f}$$

$$\boldsymbol{v}(\boldsymbol{x}^{\rm lb})^\top\le\boldsymbol{A}\le\boldsymbol{v}(\boldsymbol{x}^{\rm ub})^\top \tag{4g}$$

where $\boldsymbol{M}\succ 0$ and $\boldsymbol{N}\succ 0$ are arbitrary basis matrices to be designed later. $\{\boldsymbol{d}_1,\ldots,\boldsymbol{d}_L\}$ are the standard basis vectors in $\mathbb{R}^{|\mathcal{L}|}$. $\boldsymbol{v}_0$ and $\boldsymbol{x}_0$ are the initial guesses for the elements of the voltage and the line-status vectors. They are chosen as the nominal voltage value, $\mathbf{1}$ per-unit and $\mathbf{1}_n$, respectively, to satisfy flat start operating conditions and imply a fully-connected network.

Notice that the bi-linear term $\boldsymbol{v}\boldsymbol{x}^\top$ in (3c) is replaced by $\boldsymbol{A}$ in (4c) and, therefore, we are dealing with a linear constraint. The nuclear norm term, $\|\boldsymbol{A}-\boldsymbol{v}\boldsymbol{x}^\top\|_*$, implicitly imposes the non-convex equality $\boldsymbol{A}\triangleq\boldsymbol{v}\boldsymbol{x}^\top$ by penalizing the difference.

Proposition 1: Let $\boldsymbol{v}^*$ and $\boldsymbol{x}^*$ be the solution to (3), and define $\boldsymbol{A}^*\triangleq\boldsymbol{v}^*\boldsymbol{x}^{*\top}$. The constraints in (4d), (4e), and (4g) are valid for $\boldsymbol{A}$, $\boldsymbol{v}$, and $\boldsymbol{x}^\top$.

Proof: Consider arbitrary voltage and line-status vectors $\boldsymbol{v}$ and $\boldsymbol{x}$, respectively. Let $\boldsymbol{v}^*$ and $\boldsymbol{x}^*$ be the solutions to (3), when voltage and current-injection measurements are chosen from the sets $\mathcal{S}_v$ and $\mathcal{S}_i$, respectively. Constraint (4d) becomes

$$\boldsymbol{e}_k^\top\boldsymbol{A}^*=\boldsymbol{e}_k^\top\boldsymbol{v}^*\boldsymbol{x}^\top=v_k\boldsymbol{x}^\top \qquad \forall k\in\mathcal{S}_v. \tag{5}$$

This implies that the constraint (4d) holds for any given $k\in\mathcal{N}$. For every $l\in\mathcal{L}$, (4e) leads to the following equality

$$\boldsymbol{A}^*\boldsymbol{d}_l^\top=\boldsymbol{v}^*\boldsymbol{x}^\top\boldsymbol{d}_l^\top=\boldsymbol{v}x_l \qquad \forall l\in\mathcal{S}_x, \tag{6}$$

where it shows that $\boldsymbol{v}x_l$ becomes equivalent to (4e). Similarly, for every $k\in\mathcal{N}$ and $l\in\mathcal{L}$, (4g) becomes

$$x_l{}^{\rm lb}\le\ x_l{}^*\ \le x_l{}^{\rm ub}, \tag{7a}$$

$$\Rightarrow\ v_k{}^*x_l{}^{\rm lb}\le v_k{}^*x_l{}^*\le v_k{}^*x_l{}^{\rm ub}, \tag{7b}$$

$$\Rightarrow\ v_k{}^*x_l{}^{\rm lb}\le\ A_{kl}{}^*\ \le v_k{}^*x_l{}^{\rm ub}. \tag{7c}$$

Note that (4g), (7b), and (7c) are equivalent. Equations (5), (6), and (7) complete the proof for the valid inequalities in (4). ■

Remark 1: Observe that the nuclear norm term in (4a), $\|\boldsymbol{A}-\boldsymbol{v}\boldsymbol{x}^\top\|_*$ is non-convex. The inertia terms $\|\boldsymbol{v}-\boldsymbol{v}_0\|^2_{\boldsymbol{M}}$ and $\|\boldsymbol{x}-\boldsymbol{x}_0\|^2_{\boldsymbol{N}}$ are added to convexify the overall objective function. This is formally stated by the following theorem.

Remark 2: The presence of matrices $\boldsymbol{M}$ and $\boldsymbol{N}$ indicates that the choice of basis can be arbitrary. We will demonstrate how $\boldsymbol{M}$ and $\boldsymbol{N}$ can boost the convergence rate of the proposed approach. A penalty term induced by a physical quantity, such as loss, can help address the non-convexity.

Theorem 1: The function $f:\mathbb{R}^{n\times l}\times\mathbb{R}^n\times\mathbb{R}^l\to\mathbb{R}$, defined as

$$\begin{aligned}f(\boldsymbol{A},\boldsymbol{v},\boldsymbol{x})\triangleq&\|\boldsymbol{M}^{\frac{1}{2}}(\boldsymbol{A}-\boldsymbol{v}\boldsymbol{x}^\top)\boldsymbol{N}^{\frac{1}{2}}\|_*\\&+\|\boldsymbol{v}-\boldsymbol{v}_0\|^2_{\boldsymbol{M}}+\|\boldsymbol{x}-\boldsymbol{x}_0\|^2_{\boldsymbol{N}},\end{aligned} \tag{8}$$

is convex.

Proof: Define new variables $\boldsymbol{B}\triangleq\boldsymbol{M}^{\frac{1}{2}}\boldsymbol{A}\boldsymbol{N}^{\frac{1}{2}}$, $\boldsymbol{s}\triangleq\boldsymbol{M}^{\frac{1}{2}}\boldsymbol{v}$, and $\boldsymbol{r}\triangleq\boldsymbol{N}^{\frac{1}{2}}\boldsymbol{x}$. It suffices to show that the following function is convex:

$$g(\boldsymbol{B},\boldsymbol{s},\boldsymbol{r})\triangleq\|\boldsymbol{B}-\boldsymbol{s}\boldsymbol{r}^\top\|_*+\|\boldsymbol{s}\|_2^2+\|\boldsymbol{r}\|_2^2. \tag{9}$$

According to triangle inequality we have:

$$g(\boldsymbol{\Lambda},\boldsymbol{\nu},\boldsymbol{\xi})-\theta g(\boldsymbol{B}_1,\boldsymbol{s}_1,\boldsymbol{r}_1)-(1-\theta)g(\boldsymbol{B}_2,\boldsymbol{s}_2,\boldsymbol{r}_2)\le 0, \tag{10}$$

where $\boldsymbol{\Lambda}$, $\boldsymbol{\nu}$, and $\boldsymbol{\xi}$ are

$$\boldsymbol{\Lambda}=\theta\boldsymbol{B}_1+(1-\theta)\boldsymbol{B}_2, \tag{11a}$$

$$\boldsymbol{\nu}=\theta\boldsymbol{s}_1+(1-\theta)\boldsymbol{s}_2, \tag{11b}$$

$$\boldsymbol{\xi}=\theta\boldsymbol{r}_1+(1-\theta)\boldsymbol{r}_2. \tag{11c}$$

The inequality in (10) can be expanded as

$$\begin{aligned}\|\boldsymbol{\Lambda}-[\boldsymbol{\nu}][\boldsymbol{\xi}]^\top\|_*-\theta\|\boldsymbol{B}_1-\boldsymbol{s}_1\boldsymbol{r}_1^\top\|_*-(1-\theta)\|\boldsymbol{B}_2-\boldsymbol{s}_2\boldsymbol{r}_2^\top\|_* \\ \leq \|\theta\boldsymbol{s}_1\boldsymbol{r}_1^\top+(1-\theta)\boldsymbol{s}_2\boldsymbol{r}_2^\top-[\boldsymbol{\nu}][\boldsymbol{\xi}]^\top\|_* \\ =\theta(1-\theta)\|\boldsymbol{s}_1-\boldsymbol{s}_2\|_2\|\boldsymbol{r}_1-\boldsymbol{r}_2\|_2. \qquad (12)\end{aligned}$$

Further simplification of (12) leads to

$$\begin{aligned}\|\boldsymbol{\nu}\|_2^2+\|\boldsymbol{\xi}\|_2^2-\theta(\|\boldsymbol{s}_1\|_2^2+\|\boldsymbol{r}_1\|_2^2)-(1-\theta)(\|\boldsymbol{s}_2\|_2^2+\|\boldsymbol{r}_2\|_2^2) \\ =-\theta(1-\theta)[\|\boldsymbol{s}_1-\boldsymbol{s}_2\|_2^2+\|\boldsymbol{r}_1-\boldsymbol{r}_2\|_2^2], \qquad (13)\end{aligned}$$

which completes the proof of *Theorem 1*. ■

C. The Choice of Basis Matrices

The original problem in (3) has been expressed as a convex optimization problem (4) with basis matrices $\boldsymbol{M}$ and $\boldsymbol{N}$. These basis matrices should be chosen properly such that the solution to (4) satisfies the problem in (3). Inspired by [19], matrix $\boldsymbol{M}$ is chosen to represent the network's total power loss.

Power flow on a line $l \in \mathcal{L}$ can be calculated for the two neighboring buses $(i, j) \in \mathcal{N}$ as

$$\vec{p}_l = v_i(v_i - v_j)g_l x_l, \qquad (14a)$$

$$\overleftarrow{p}_l = v_j(v_j - v_i)g_l x_l, \qquad (14b)$$

where $\vec{p}_l$ and $\overleftarrow{p}_l$ denote the power flow from the starting and ending sides of each line $l \in \mathcal{L}$. Power loss on a line is

$$\begin{aligned}\vec{p}_l+\overleftarrow{p}_l &= v_i(v_i-v_j)g_lx_l+v_j(v_j-v_i)g_lx_l && (15a)\\ &= ({v_i}^2-v_iv_j+{v_j}^2-v_iv_j)g_lx_l && (15b)\\ &= ({v_i}^2+{v_j}^2-2v_iv_j)g_lx_l && (15c)\\ &= (v_i-v_j)(g_lx_l)(v_i-v_j)^\top. && (15d)\end{aligned}$$

The total power loss is the sum of power flows entering the lines through their starting and ending buses as

$$\vec{\boldsymbol{p}} = \mathrm{diag}\{\vec{\boldsymbol{L}}\,\boldsymbol{v}\,\boldsymbol{v}^\top\,\vec{\boldsymbol{G}}^\top\}, \quad \overleftarrow{\boldsymbol{p}} = \mathrm{diag}\{\overleftarrow{\boldsymbol{L}}\,\boldsymbol{v}\,\boldsymbol{v}^\top\,\overleftarrow{\boldsymbol{G}}^\top\} \qquad (16a)$$

$$\sum(\vec{\boldsymbol{p}}+\overleftarrow{\boldsymbol{p}}) = Tr(\boldsymbol{v}\,\boldsymbol{v}^\top(\vec{\boldsymbol{G}}^\top\,\vec{\boldsymbol{L}}+\overleftarrow{\boldsymbol{G}}^\top\,\overleftarrow{\boldsymbol{L}})) \qquad (16b)$$

$$= \boldsymbol{v}^\top\,(\vec{\boldsymbol{G}}^\top\,\vec{\boldsymbol{L}}+\overleftarrow{\boldsymbol{G}}^\top\,\overleftarrow{\boldsymbol{L}})\,\boldsymbol{v}. \qquad (16c)$$

Using (16c), we can choose $\boldsymbol{M}$ as

$$\boldsymbol{M} = (\vec{\boldsymbol{G}}^\top\,\vec{\boldsymbol{L}}+\overleftarrow{\boldsymbol{G}}^\top\,\overleftarrow{\boldsymbol{L}}). \qquad (17)$$

Notice that if $\boldsymbol{M}$ is chosen as in (17), which is actually equal to the conductance matrix $\boldsymbol{G}$, loss minimization will be indirectly embedded in the objective function (4a) with a proper choice of $\boldsymbol{N}$. $\boldsymbol{N} = \boldsymbol{I}_{l\times l}$ implicitly penalizes the power loss over all the lines as given in (15).

D. Strengthening the Convex Relaxation

Power networks usually have intermediate buses (or hidden nodes [20]) that do not demand/supply power or current with any external source or load, e.g., see bus 3 in Fig. 1. These intermediate buses are referred to as *zero injection buses* [41]. We exploit their presence to define a number of valid inequality and strengthen the convex relaxation in (4).

Definition 1: A bus $k \in \mathcal{N}$ is regarded as a zero injection bus if both power and current injections at bus k are zero, i.e.,if no load or source is located at the bus [19]. The set of zero injection buses are presented by $\mathcal{Z}$.

Define $\boldsymbol{v}^*$ and $\boldsymbol{x}^*$ be the solutions to the original problem (3). Then,

$$\boldsymbol{e}_k^\top \mathrm{diag}\{\boldsymbol{G}\boldsymbol{v}^*\boldsymbol{x}^{*\top}\} = \boldsymbol{0}_n \qquad (18)$$

holds for every $k \in \mathcal{Z}$, where $n = |\mathcal{Z}|$.

For zero injection buses, the sum of the currents absorbed from the distribution network is equal to the sum of the currents they supply to the distribution network. This feature can be expressed as

$$\begin{aligned}&\boldsymbol{e}_k^\top \mathrm{diag}\{\boldsymbol{G}\boldsymbol{v}^*\boldsymbol{x}^{*\top}\} = \\ &\sum_{l=1}^{|\mathcal{K}|} d_l^\top(\vec{\boldsymbol{L}}\,\mathrm{diag}\{\vec{\boldsymbol{G}}\boldsymbol{v}^*\boldsymbol{x}^{*\top}\}+\overleftarrow{\boldsymbol{L}}\,\mathrm{diag}\{\overleftarrow{\boldsymbol{G}}\boldsymbol{v}^*\boldsymbol{x}^{*\top}\}), \qquad (19)\end{aligned}$$

where $\mathcal{K}$ is the set of neighbor buses of the zero injection bus k. The following formulation can be inferred from (19)

$$\begin{aligned}&\sum_{l=1}^{|\mathcal{K}|} d_l^\top(\vec{\boldsymbol{L}}\,\mathrm{diag}\{\vec{\boldsymbol{G}}\boldsymbol{v}^*\boldsymbol{x}^{*\top}\}) \\ &\qquad = -\sum_{l=1}^{|\mathcal{K}|} d_l^\top(\overleftarrow{\boldsymbol{L}}\,\mathrm{diag}\{\overleftarrow{\boldsymbol{G}}\boldsymbol{v}^*\boldsymbol{x}^{*\top}\}), \qquad (20)\end{aligned}$$

concluding that (18) is valid for any $k \in \mathcal{Z}$.

According to (20), the set of additional constraints

$$\boldsymbol{e}_k^\top \mathrm{diag}\{\boldsymbol{G}\boldsymbol{A}\} = \boldsymbol{0}_n \qquad (21)$$

can be added in (4) to strengthen its relaxation.

E. Joint Observation in the Presence of Noisy Measurements

The convex problem (4) can become infeasible, or result in a poor approximate, if available measurements become noisy. In this case, solving the state estimation problem requires tackling two concerns: (i) how to address nonlinear relation between sensor measurements and state variables, (ii) how to address corrupted sensor measurements. We introduce auxiliary variables $\boldsymbol{v}^{\mathrm{g}}, \boldsymbol{i}^{\mathrm{g}} \in \mathbb{R}^{|\mathcal{N}|}$, $\vec{\boldsymbol{i}}^{\mathrm{g}}, \overleftarrow{\boldsymbol{i}}^{\mathrm{g}} \in \mathbb{R}^{|\mathcal{L}|}$ and $\boldsymbol{v}^{\mathrm{s}}, \boldsymbol{i}^{\mathrm{s}} \in \mathbb{R}^{|\mathcal{N}|}$, $\vec{\boldsymbol{i}}^{\mathrm{s}}, \overleftarrow{\boldsymbol{i}}^{\mathrm{s}} \in \mathbb{R}^{|\mathcal{L}|}$ to handle measurement noise where they account for Gaussian and sparse noise estimations, respectively. New variables $\boldsymbol{u} \in \mathbb{R}^{|\mathcal{N}|}$ and $\boldsymbol{S} \in \mathbb{R}^{|\mathcal{N}|\times|\mathcal{L}|}$ account for the $\boldsymbol{v}^{\mathrm{g}^2}$ and $\boldsymbol{v}^{\mathrm{s}}\boldsymbol{x}^\top$, respectively. Unknown measurement noise can be estimated by incorporating these auxiliary variables as convex regularization terms into the objective function (4a). The joint state estimation and topology

identification problem, that is robust to noisy and entirely corrupted measurements, can be formulated as

$$\begin{aligned}
\underset{\substack{\boldsymbol{A}\in\mathbb{R}^{|\mathcal{N}|\times|\mathcal{L}|}\\ \boldsymbol{S}\in\mathbb{R}^{|\mathcal{N}|\times|\mathcal{L}|}\\ \boldsymbol{i}^{\mathrm{g}},\boldsymbol{i}^{\mathrm{s}}\in\mathbb{R}^{|\mathcal{N}|}\\ \boldsymbol{u},\boldsymbol{v},\boldsymbol{v}^{\mathrm{g}},\boldsymbol{v}^{\mathrm{s}}\in\mathbb{R}^{|\mathcal{N}|}\\ \boldsymbol{x},\vec{\boldsymbol{i}}^{\mathrm{g}},\vec{\boldsymbol{i}}^{\mathrm{s}},\overleftarrow{\boldsymbol{i}}^{\mathrm{g}},\overleftarrow{\boldsymbol{i}}^{\mathrm{s}}\in\mathbb{R}^{|\mathcal{L}|}}}{\text{minimize}} \quad & \|\boldsymbol{M}^{\frac{1}{2}}(\boldsymbol{A}-\boldsymbol{v}\boldsymbol{x}^{\top})\boldsymbol{N}^{\frac{1}{2}}\|_{*}+\|\boldsymbol{v}-\boldsymbol{v}_0\|^2_{\boldsymbol{M}}\\
&+\|\boldsymbol{x}-\boldsymbol{x}_0\|^2_{\boldsymbol{N}}\\
&+\mu_1(\boldsymbol{1}^{\top}\boldsymbol{u})+\mu_2||\boldsymbol{i}^{\mathrm{g}}||_2^2+\mu_3||\boldsymbol{v}^{\mathrm{s}}||_2^2\\
&+\mu_4||\boldsymbol{i}^{\mathrm{s}}||_2^2+\mu_5||\boldsymbol{S}||_{*} \qquad (22a)\\
&+\mu_6||\vec{\boldsymbol{i}}^{\mathrm{g}}||_2^2+\mu_7||\vec{\boldsymbol{i}}^{\mathrm{s}}||_2^2\\
&+\mu_8||\overleftarrow{\boldsymbol{i}}^{\mathrm{g}}||_2^2+\mu_9||\overleftarrow{\boldsymbol{i}}^{\mathrm{s}}||_2^2
\end{aligned}$$

$$\text{subject to} \quad v_k=\hat{v}_k-v_k^g-v_k^s \qquad \forall k\in\mathcal{S}_v \quad (22b)$$

$$\boldsymbol{e}_k^{\top}\mathrm{diag}\{\boldsymbol{G}\boldsymbol{A}\}=\hat{\imath}_k-i_k^g-i_k^s \qquad \forall k\in\mathcal{S}_i \quad (22c)$$

$$\boldsymbol{d}_l\mathrm{diag}\{\vec{\boldsymbol{G}}\boldsymbol{A}\}=\vec{\imath}_k-\vec{\imath}_k^g-\vec{\imath}_k^s \qquad \forall l\in\mathcal{S}_{\vec{\imath}} \quad (22d)$$

$$\boldsymbol{d}_l\mathrm{diag}\{\overleftarrow{\boldsymbol{G}}\boldsymbol{A}\}=\overleftarrow{\imath}_k-\overleftarrow{\imath}_k^g-\overleftarrow{\imath}_k^s \qquad \forall l\in\mathcal{S}_{\overleftarrow{\imath}} \quad (22e)$$

$$\boldsymbol{A}\,\boldsymbol{d}_l^{\top}=\boldsymbol{v}\,\hat{x}_l \qquad \forall l\in\mathcal{S}_x \quad (22f)$$

$$\boldsymbol{S}\,\boldsymbol{d}_l^{\top}=\boldsymbol{v}^{\mathrm{s}}\,\hat{x}_l \qquad \forall l\in\mathcal{S}_x \quad (22g)$$

$$\boldsymbol{x}^{\mathrm{lb}}\le\boldsymbol{x}\le\boldsymbol{x}^{\mathrm{ub}} \quad (22h)$$

$$\boldsymbol{v}(\boldsymbol{x}^{\mathrm{lb}})^{\top}\le\boldsymbol{A}\le\boldsymbol{v}(\boldsymbol{x}^{\mathrm{ub}})^{\top} \quad (22i)$$

$$\boldsymbol{v}^{\mathrm{s}}(\boldsymbol{x}^{\mathrm{lb}})^{\top}\le\boldsymbol{S}\le\boldsymbol{v}^{\mathrm{s}}(\boldsymbol{x}^{\mathrm{ub}})^{\top} \quad (22j)$$

$$v_k^{g2}\le u_k \qquad \forall k\in\mathcal{S}_v \quad (22k)$$

$$\begin{bmatrix} x_l & \hat{v}_k x_l-A_{kl}-S_{kl}\\ \hat{v}_k x_l-A_{kl}-S_{kl} & u_k\end{bmatrix}\succeq 0 \qquad \forall k\in\mathcal{S}_v,\ \forall l\in\mathcal{L} \quad (22l)$$

where $\mu_n\ge 0$ are pre-selected coefficients for every $n=\{1,2,\ldots 9\}$ that balance the data fitting cost $\mu_1(\boldsymbol{1}^{\top}\boldsymbol{u})+\mu_2||\boldsymbol{i}^{\mathrm{g}}||_2^2+\mu_3||\boldsymbol{v}^{\mathrm{s}}||_2^2+\mu_4||\boldsymbol{i}^{\mathrm{s}}||_2^2+\mu_5||\boldsymbol{S}||_{*}+\mu_6||\vec{\boldsymbol{i}}^{\mathrm{g}}||_2^2+\mu_7||\vec{\boldsymbol{i}}^{\mathrm{s}}||_2^2+\mu_8||\overleftarrow{\boldsymbol{i}}^{\mathrm{g}}||_2^2+\mu_9||\overleftarrow{\boldsymbol{i}}^{\mathrm{s}}||_2^2$ with the remaining elements of the objective function in (22a). $\mathcal{S}_{\vec{\imath}}$ and $\mathcal{S}_{\overleftarrow{\imath}}$ denote the set of current flow measurements from both sides of each line. The objective function (4a) aims to handle the nonlinearity of the measurement equation, while the convex regularization term added in (22a) deals with the noisy and corrupted measurements.

Proposition 2: Let $\boldsymbol{v}^*$, $\boldsymbol{x}^*$, $\boldsymbol{v}^{\mathrm{g}^*}$, $\boldsymbol{i}^{\mathrm{g}^*}$, $\vec{\boldsymbol{i}}^{\mathrm{g}^*}$, $\overleftarrow{\boldsymbol{i}}^{\mathrm{g}^*}$, $\boldsymbol{v}^{\mathrm{s}^*}$, $\boldsymbol{i}^{\mathrm{s}^*}$, $\vec{\boldsymbol{i}}^{\mathrm{s}^*}$, $\overleftarrow{\boldsymbol{i}}^{\mathrm{s}^*}$, and $\boldsymbol{u}^*$ be the ground-truth values for the original problem (3). Let $\boldsymbol{u}^*\triangleq\boldsymbol{v}^{\mathrm{g}^*2}$, $\boldsymbol{S}^*\triangleq\boldsymbol{v}^{\mathrm{s}}\boldsymbol{x}^{\top}$, and $\boldsymbol{A}^*\triangleq\boldsymbol{v}^*\boldsymbol{x}^{*\top}$. Then, the constraint (22l) is satisfied.

Proof: Since v_k^* and x_l^* are positive, one can write

$$\begin{aligned}
A_{kl}^*=v_k^*x_l^* \;&\Leftrightarrow A_{kl}^*=(\hat{v}_k-v_k^{g^*}-v_k^{s^*})x_l^* && (23a)\\
&\Rightarrow\ \hat{v}_kx_l^*-A_{kl}^* \;\;=(v_k^{g^*}+v_k^{s^*})x_l^*\\
&\Rightarrow\ \hat{v}_kx_l^*-A_{kl}^*-S_{kl}^* \;\;=v_k^{g^*}x_l^*\\
&\Leftrightarrow(\hat{v}_kx_l^*-A_{kl}^*-S_{kl}^*)^2=(v_k^{g^*})^2\,{x_l}^{*2} && (23b)\\
&\Rightarrow(\hat{v}_kx_l^*-A_{kl}^*-S_{kl}^*)^2=u_k^*x_l^* \text{ or } 0\\
&\Leftrightarrow(\hat{v}_kx_l^*-A_{kl}^*-S_{kl}^*)^2\le u_k^*x_l^* \text{ or } 0 && (23c)
\end{aligned}$$

As seen, (23) is equivalent to (22l) under the proposition 2. This completes the proof. ■

If pre-selected coefficients are chosen as $\mu_n=0$, the objective function (22a) is reduced to the objective function (4a), which can only contrive the non-convexity of the measurement equations in noiseless scenarios. If $\mu_n=+\infty$, then the objective function (22a) prioritizes estimating the unknown noise values while ignoring the remaining elements.

Remark 3: If the relaxation is exact, then we have $\boldsymbol{A}^*=\boldsymbol{v}^*\boldsymbol{x}^{*\top}$, in which case the solver only minimizes the error values, $\mu_1(\boldsymbol{1}^{\top}\boldsymbol{u})+\mu_2||\boldsymbol{i}^{\mathrm{g}}||_2^2+\mu_3||\boldsymbol{v}^{\mathrm{s}}||_2^2+\mu_4||\boldsymbol{i}^{\mathrm{s}}||_2^2+\mu_5||\boldsymbol{S}||_{*}+\mu_6||\vec{\boldsymbol{i}}^{\mathrm{g}}||_2^2+\mu_7||\vec{\boldsymbol{i}}^{\mathrm{s}}||_2^2+\mu_8||\overleftarrow{\boldsymbol{i}}^{\mathrm{g}}||_2^2+\mu_9||\overleftarrow{\boldsymbol{i}}^{\mathrm{s}}||_2^2$, within the space of zero residual points (i.e., the set of all points that satisfy $\boldsymbol{A}=\boldsymbol{v}\boldsymbol{x}^{\top}$). Observe that $\boldsymbol{A}=\boldsymbol{v}\boldsymbol{x}^{\top}$ cannot be imposed as a constraint due to its non-convexity. This is the motivation behind incorporating its surrogate into the objective. However, this surrogate will ultimately serve as a hard constraint.

The goal of (22) is to determine an approximate solution for the state estimation problem in the presence of noisy measurements without increasing the number of available sensor, or for the joint state estimation and topology identification problem despite noisy and entirely corrupted measurements with the help of additional set of measurements. It should be noted that corrupted measurements can make the network unobservable, and the number of available sensors should be relatively high (i.e., $\Theta\ge 4\Upsilon$-4, where Θ and Υ denote the total number of available sensors and the state variables to be found, respectively) for a robust estimation [7]. If one considers a joint state estimation and topology identification problem in the presence of noise and severely corrupted measurements, the number of unknown parameters could grow beyond the number of possible measurements. This makes the problem unsolvable due to information-theoretic limitations [7].

IV. Case Studies

In the following, standard IEEE AC benchmarks are transformed into DC benchmarks by substituting AC generators with DC sources coupled with buck converters, and having

distribution lines purely resistive. While the standardization of future DC networks is under development, IEEE [42], European standard ETSI [43], EMerge Alliance [44], and IEC SG4 [45] have suggested 380 V DC as a suitable rated voltage level for distribution systems. Herein, the DC distribution line parameters are adjusted according to the rated voltage level [46], [47]. All lines are equipped with switches to control the network topology. If monitored, a bus is equipped with a sensor to measure voltage and/or a sensor to measure current injection. Monitored lines refer to the lines with a sensor. The optimization problem is run using the conic interior-point solver, MOSEK [48], in the CVX [49] optimization package.

A. Numerical Studies

The joint state estimation and topology identification problem is examined for the modified IEEE 9-bus [50], 14-bus [51], and 30-bus systems [52] when measurements are assumed noiseless. We compare our method in (4), using proper basis $\boldsymbol{M}$ and $\boldsymbol{N}$ values in (17) and the set of additional constraints in (21), with the conventional GSE method [4]. Herein, the total number of sensors is initially determined such that the jacobian matrix of estimation equations [4] is surely not full rank while initial configuration of sensors is randomly chosen. Then, the number of sensors is gradually increasing to observe the performances of both proposed method and the method in [4] for varying numbers and locations of sensors.

For a specified number of sensors, the sensors are randomly deployed. This configuration is simulated for a time horizon with 100 steps while random changes in voltage levels and an arbitrary line removal happen at every time-step and every fifth time-step, respectively. Afterward, the sensor configuration is randomly rearranged without increasing the number of sensors, and then the simulation is run again. To provide more reliable statistical results, for a given number of sensors, this process is repeated 250 times. Each approach has a flat start with 10^{-6} as the mismatch threshold to conclude a successful run. The success rate percentage is computed as $\nu^i = \frac{1}{c}\sum_1^c \frac{h_c^i - f_c^i}{h_c^i} \times 100$, where h_c^i, and f_c^i, are the number of steps in a horizon, and the number of steps failed to satisfy the mismatch threshold in a horizon, respectively. c, and i denote the number of random attempts for sensor reconfiguration, and the total number of sensors, respectively. In this study, $h_c^i = 100$ for every $c \in \{1, 2, \ldots 250\}$.

It should be noted that the network observability is determined by both the number and the location of sensors. The success of the GSE method hinges on a full observability condition that would require highly-redundant sensor allocation. As seen in Fig. 2(a)–(c), the proposed method significantly outperforms the GSE approach.

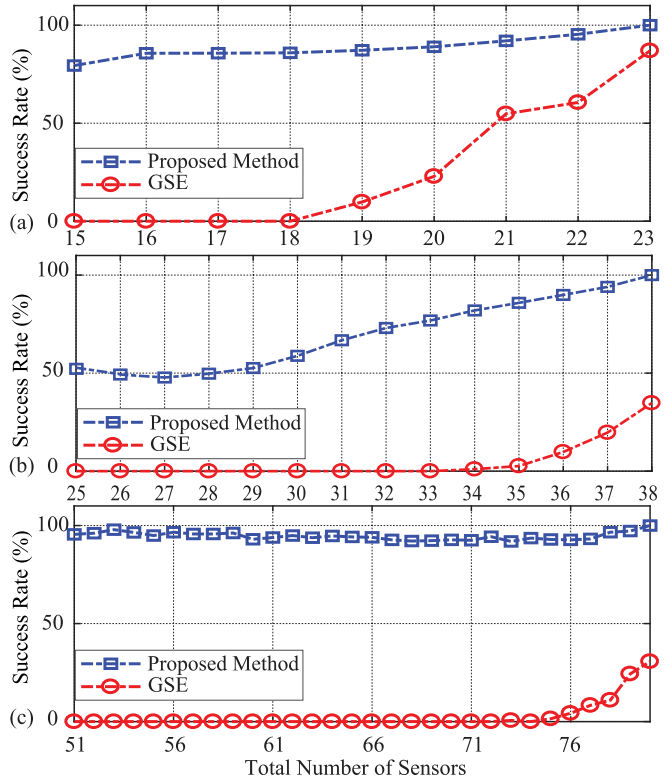

Fig. 2. Comparative convergence rates of proposed and generalized state estimation methods for the IEEE (a) 9-bus, (b) 14-bus, and (c) 30 bus systems.

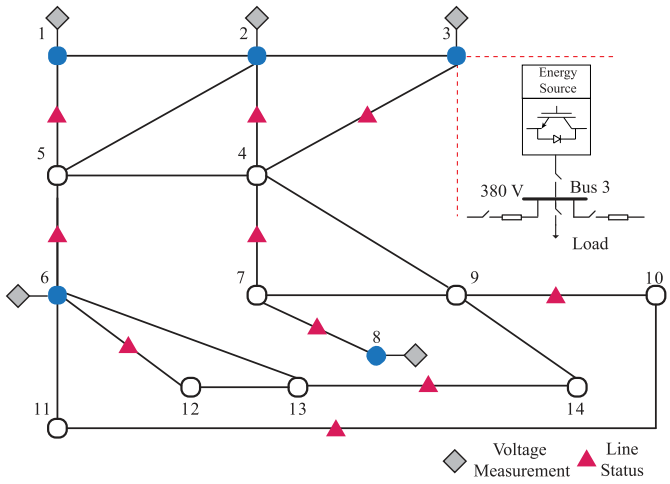

Fig. 3. The modified IEEE 14-bus system populated with 5 DC-DC buck converters (illustrated by ●), and equipped with sensors to monitor voltages (illustrated by ◇), line statuses (illustrated by ▲), and injected current at bus $k \in \mathcal{N} \setminus \{\mathcal{Z}\}$.

B. Experimental Studies

In the modified 14-bus system, the input voltage of DC-DC buck converters is 500 V, while the distribution network is rated for 380 V. The ratings of the power converters located at buses 1, 2, 3, 6, and 8 are 150 kW, 50 kW, 100 kW, 100 kW, and 50 kW, respectively. Sample consumption trajectories for the six out of eleven loads are given in Fig. 4. The consumption profiles intentionally mimic a 24-hour load pattern, and are generated using poisson distribution. This distribution assumes that the sudden load changes occur randomly with the probability mass function, $P(k) = e^{-\lambda}\frac{\lambda^k}{k!}$. Here, k and λ denote the type and average number of load changes. The voltage sensors are placed on the buses with a power converter. The current injection values are measured for buses ($\mathcal{N} \setminus \mathcal{Z}$) that are not zero-injection buses.

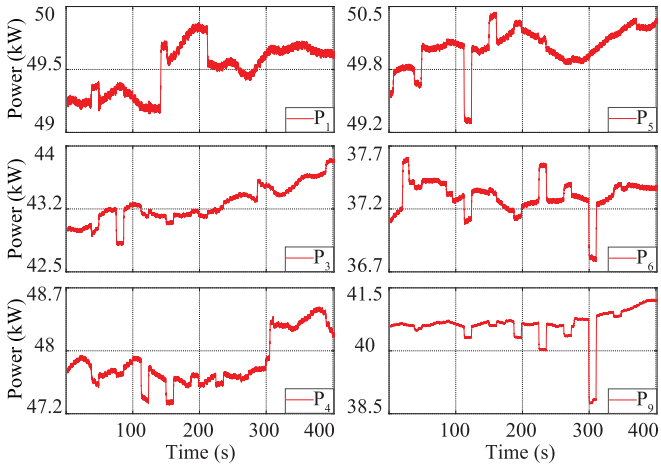

Fig. 4. Load power trajectories at selected buses 1, 3, 4, 5, 6, and 9.

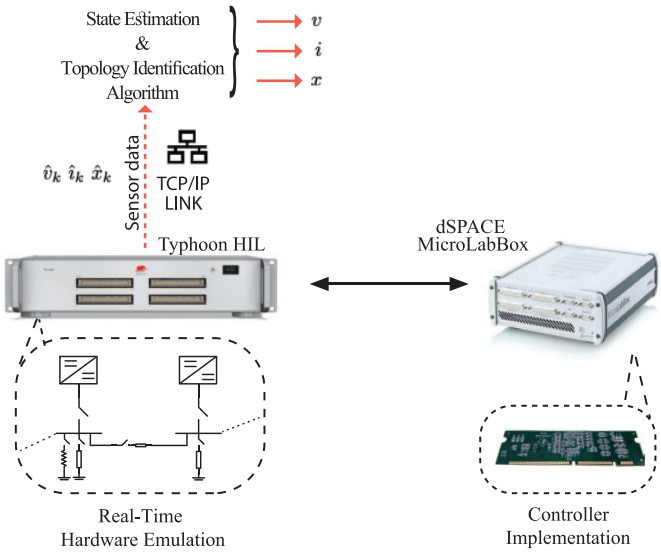

Fig. 5. DC network joint observation testbed on a HIL system embodying of controller implementation (dSPACE), real-time hardware emulation (Typhoon HIL), and TCP/IP communication link for data transfer.

It should be observed that bus 7 and bus 14 of the IEEE-14 bus system are zero injection buses. The statuses of ten lines are monitored as illustrated in Fig. 3. The internal droop mechanism of power converters regulate their output voltage in response to output power variations due to the changes in the load profile or network topology. HIL platform with a dSPACE DS1202 MicroLabBox to perform droop controllers for each converters, and a Typhoon HIL604 unit to emulate power converters and the distribution network is used to emulate this network. The proposed optimization algorithm runs on a PC with 16-core, Xeon processor and 256 GB RAM.

1) Noiseless Measurements: We consider a time horizon, where the statuses of unmonitored lines change randomly and load profiles are dynamic. The proposed formulation in (4), with $\boldsymbol{M} = \boldsymbol{G}$, $\boldsymbol{N} = \boldsymbol{I}_{l\times l}$, and the set of additional constraints in (21), finds states and topology configurations every five seconds. Fig. 6 shows the recovered (v) and the ground-truth

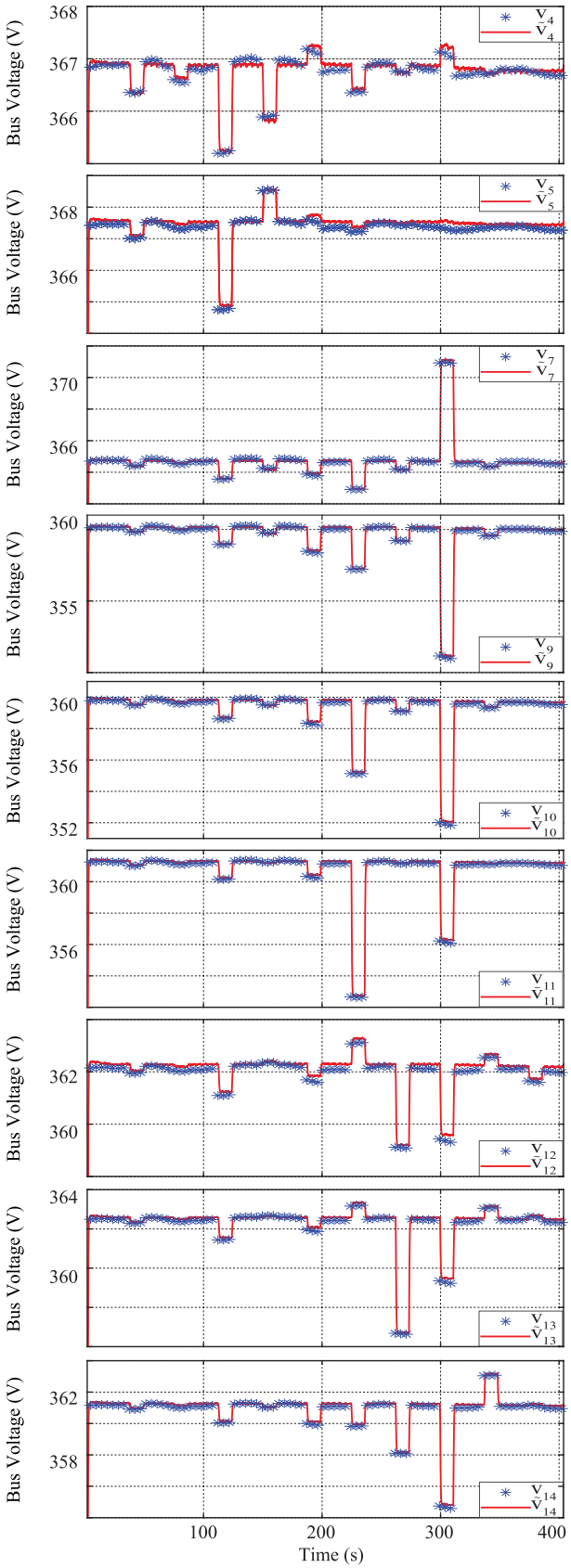

Fig. 6. Estimated (v_k), and ground-truth ($\tilde{v}_k$) voltage values for unmonitored buses.

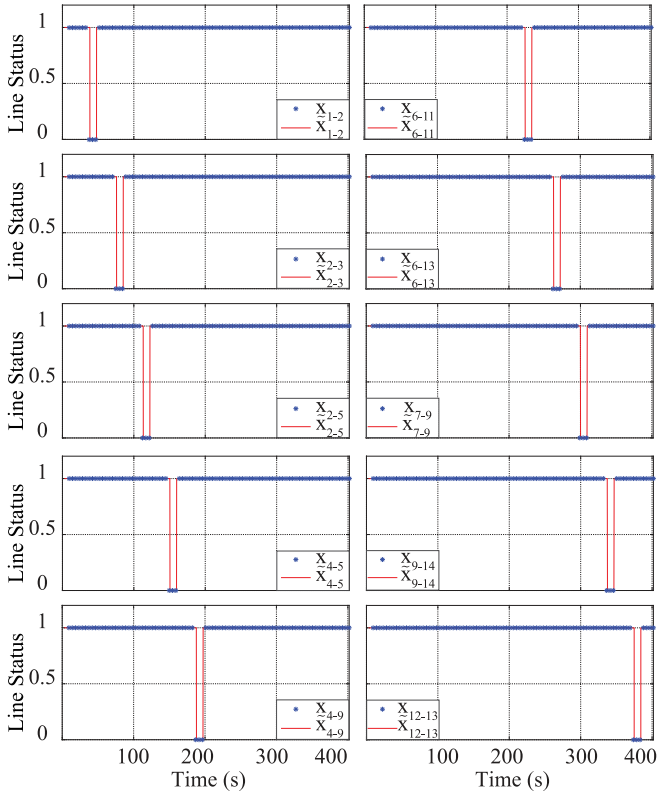

Fig. 7. Estimated (x_l), and ground-truth ($\tilde{x}_l$) values for the statuses of the lines in response to the removal of one line. x_{a-b} denotes the line status for a line which starts from node a and ends in b.

($\tilde{v}$) voltage values for the unmonitored buses. Fig. 7 presents the recovered (x) and the ground-truth ($\tilde{x}$) values for the statuses of unmonitored lines in response to the removal of an arbitrary line. It is observed that the maximum errors in terms of percentage for recovered voltage values and statuses of lines are always less than 10^{-6}. Consequently, the proposed method yields a very good pursuit of ground-truth values for voltages and statuses of the lines when measurements are assumed noiseless. So far, we haven't used any penalty term or tuning parameter in the convex program (4). The average time for finding states and topology configurations is 2.208 s.

2) Noisy Measurements: In this section, we verify that proposed algorithm is capable of finding an approximate solution in the presence of noisy measurements. All the voltage and current measurements are assumed corrupted by zero-mean Gaussian noises with 1% standard deviation of the corresponding noiseless value. The proposed formulation in (22), with $\boldsymbol{M} = \boldsymbol{G}$ and $\boldsymbol{N} = \boldsymbol{I}_{l\times l}$, finds system states every five seconds. Root-mean-square error (RMSE) is considered to assess the estimated voltages $\boldsymbol{v}$ under the zero-mean Gaussian noise that has 1% standard deviation for all the measurements. The RMSE of the $\boldsymbol{v}$ is formalized as $\psi(\boldsymbol{v}) := \|\boldsymbol{v} - \tilde{\boldsymbol{v}}\|_2/\|\tilde{\boldsymbol{v}}\|_2^2$. The pre-selected coefficients in (22), that balance the data fitting cost, are set to $\mu_1 = \mu_2 = 10^2$ and $\mu_3 = \mu_4 = \mu_5 = \mu_6 = \mu_7 = \mu_8 = \mu_9 = 1$. It should be observed that the coefficients for the current flow measurements, μ_6, μ_7, μ_8, and μ_9, are redundant since $\mathcal{S}_{\vec{i}} = \mathcal{S}_{\overleftarrow{i}} = \emptyset$.

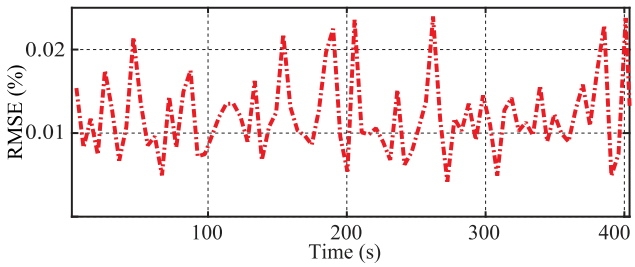

Fig. 8. The performance of (22) to estimate the vector of voltages in the case where the goal is to solve the state estimation problem in the presence of noisy measurements without increasing the number of available sensors.

a) State estimation: Herein, we demonstrate an approximate solution for the state estimation problem in the presence of noisy measurements without increasing the number of available sensors. The network topology is assumed to be either static or completely monitored due to existing noisy measurements that do not allow both state estimation and topology identification simultaneously with the same number and configuration of sensors as they are in Section IV-B1. We consider a time horizon with a dynamic load profile and a fully-monitored network topology. The RMSE of the estimated voltages for the buses with sensors, i.e., $\psi(v_k) := \|v_k - \tilde{v}_k\|_2/\|\tilde{v}_k\|_2^2$ for every $k \in \mathcal{S}_v$, shown in Fig. 8 demonstrates that an approximate solution is recoverable with 99.95% accuracy. It is observed that the maximum RMSE values for buses with and without sensors are 0.024% and 0.001%, respectively. Moreover, the maximum voltage errors, in terms of percentage for buses with and without sensors, are 0.011% and 0.0002%, respectively. Fig. 9 shows the corrupted ($\hat{v}$), recovered (v), and the ground-truth ($\tilde{v}$) voltage values where bus measurements are corrupted by 1%. The proposed method yields a very close pursuit of ground-truth voltage values when all the voltage and current measurements are subject to noise. Determination of states in the presence of noisy measurements takes 2.648 s on average.

b) State estimation and topology identification: We aim to show an approximate solution for the joint state estimation and topology identification problem with the help of additional voltage measurements. We assume that voltage measurements are available from all the buses while rest of the measurements and their configurations remain the same as they are in Section IV-B1. The experiment time horizon is considered with a random change in the statuses of unmonitored lines and dynamic load profiles. The RMSE of the estimated voltages shown in Fig. 10 demonstrates that an approximate solution is recoverable with more than 99.4% accuracy. It is observed that the maximum RMSE value for the estimated voltages is 0.543%. The maximum percentage errors for recovered voltage values and statuses of lines are less than 0.098% and 10^{-6}, respectively. Fig. 11 shows the corrupted ($\hat{v}$), recovered (v), and the ground-truth ($\tilde{v}$) voltage values for some of the selected buses. The proposed method also yields a very good pursuit of ground-truth values for line statuses same as the results shown in Fig. 7 or 14. The average time needed to find states and topology configurations in the presence of noisy measurements is 3.617 s.

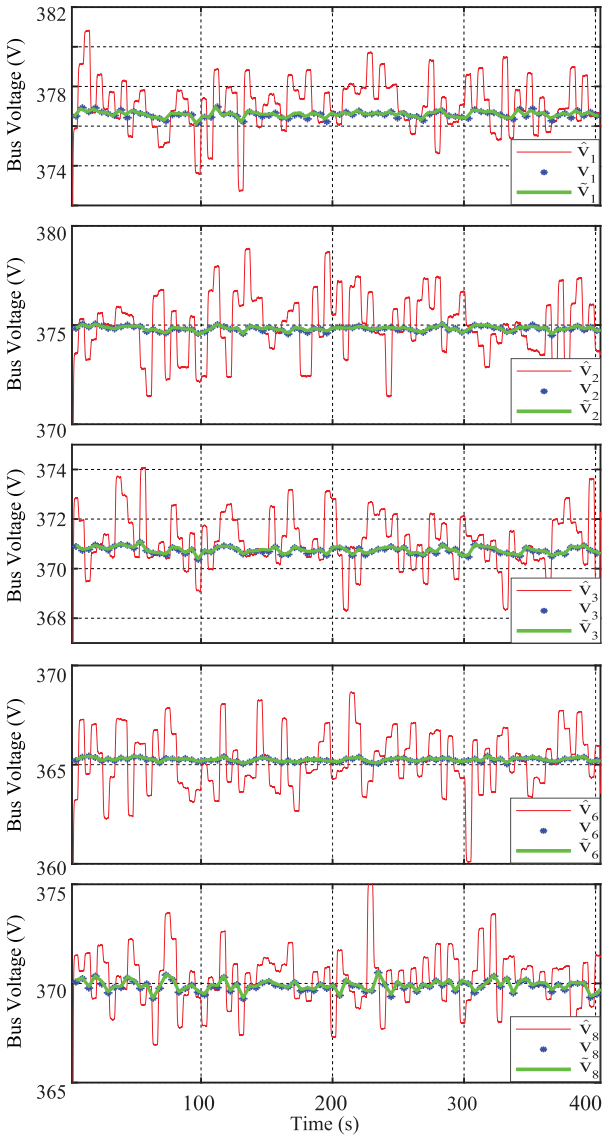

Fig. 9. Estimated voltage values obtained by (22) for the monitored sensor measurements corrupted by %1 additive noise.

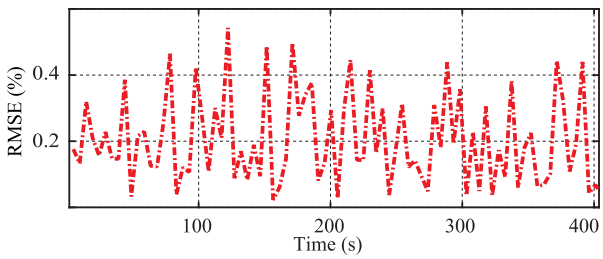

Fig. 10. The performance of (22) to estimate the vector of voltages when solving the state estimation and topology identification problem, in the presence of noisy measurements, with the help of additional voltage measurements.

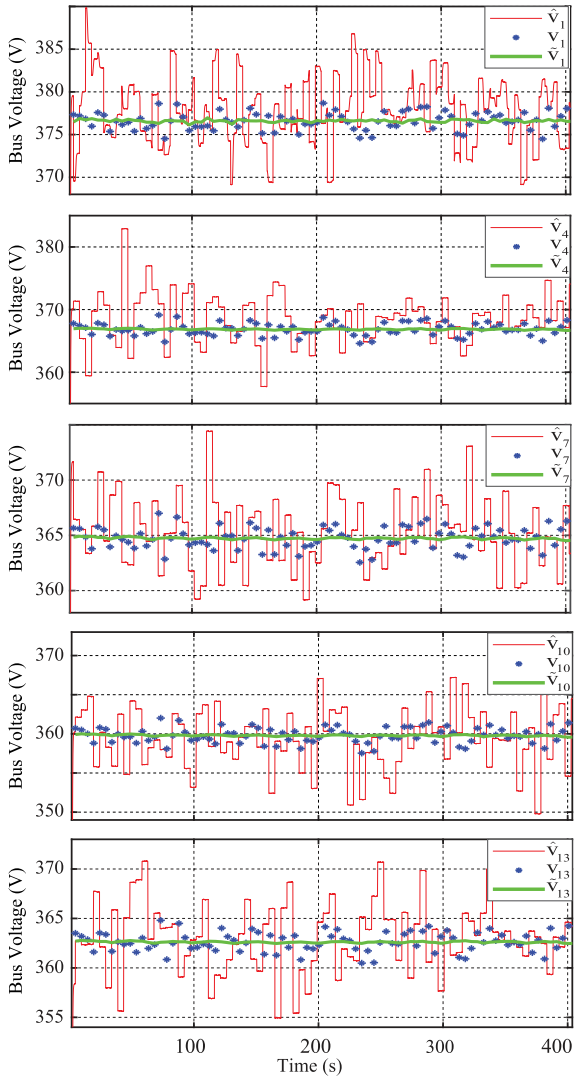

Fig. 11. Estimated voltage values obtained by (22) at selected sensor measurements. Each measurement is corrupted by %1 additive noise.

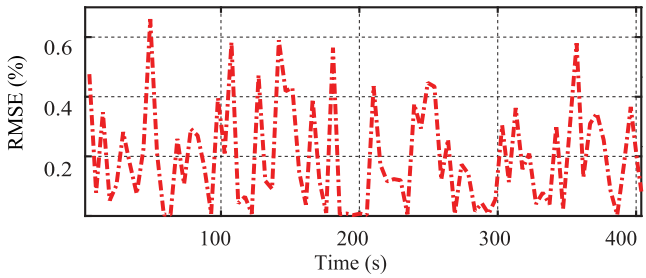

Fig. 12. The performance of (22) to estimate the vector of voltages for the modified IEEE 14-bus system where each measurement is either corrupted by zero-mean Gaussian noises with 1% standard deviation or 100% of the corresponding original value.

3) Severely Corrupted Measurements: Herein, we aim to show that the proposed method, with the help of additional set of measurements, i.e., $\mathcal{S}_{\bar{i}}$, $\mathcal{S}_{\bar{i}}$, can handle the case where each measurement is corrupted either by zero-mean Gaussian noises with 1% standard deviation or 100% of the corresponding original value. We consider a time horizon with a random change in the statuses of unmonitored lines and dynamic load profiles. The proposed formulation in (22), with $\boldsymbol{M} = \boldsymbol{G}$ and $\boldsymbol{N} = \boldsymbol{I}_{l\times l}$, finds system states every five seconds. Randomly-chosen two of the sensor measurements are severely corrupted, while the

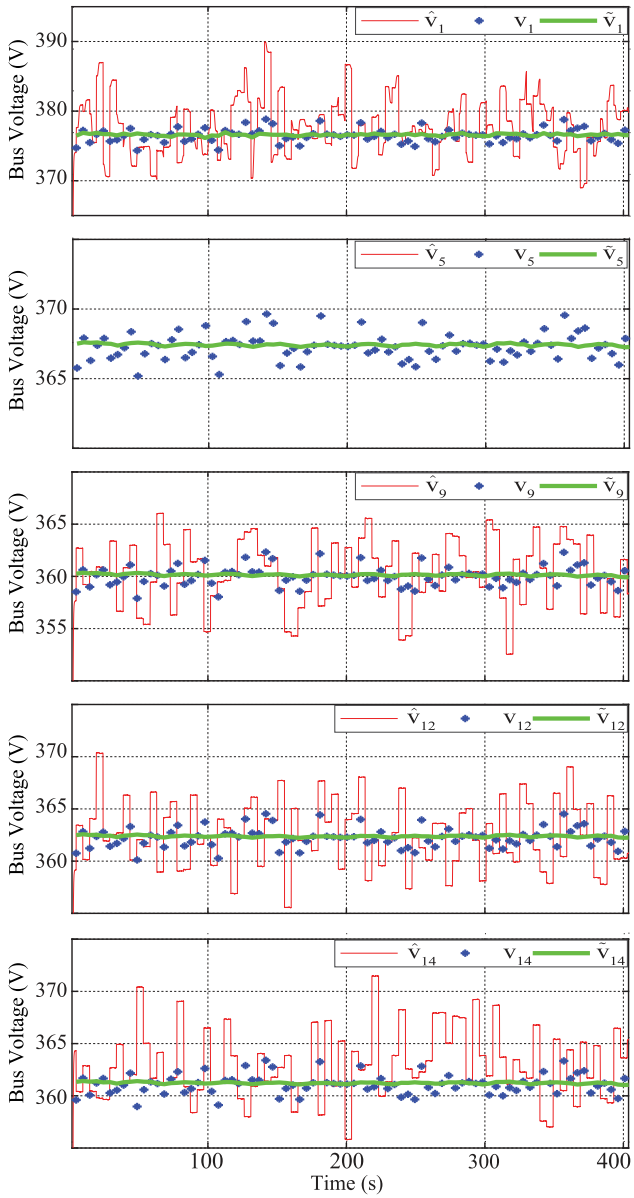

Fig. 13. Estimated voltage values obtained by (22) at selected sensor measurements. Each measurement is either corrupted by zero-mean Gaussian noises with 1% standard deviation or 100% of the corresponding original value. The voltage measurement at bus 5, $\hat{v}_5$, is out of range in Figure as it is entirely corrupted.

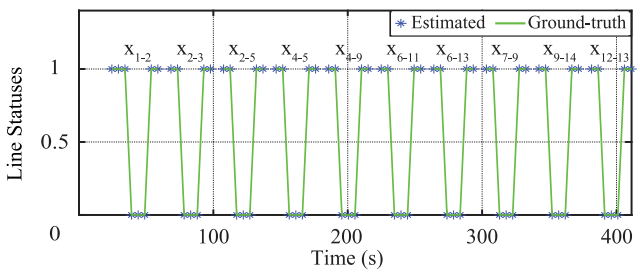

Fig. 14. Estimated (x_l), and ground-truth values, for the line statuses in response to the removal of one line. x_{a-b} denotes the status of a line starting from node a and ending in b.

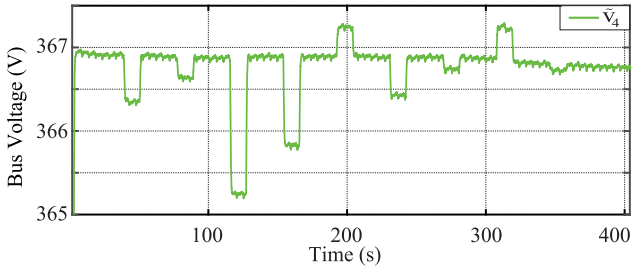

Fig. 15. Changes on the levels of ground-truth voltage values at bus 4 due to changes in topology and load power trajectories.

rest of them are under 1% Gaussian noise. These two entirely-corrupted sensors measure the voltage at bus 5 and the current injection at bus 1. Herein, the pre-selected coefficients are set to $\mu_1 = \mu_2 = 10^2$ and $\mu_3 = \mu_4 = \mu_5 = \mu_6 = \mu_7 = \mu_8 = \mu_9 = 1$. Fig. 12 demonstrates that an approximate solution is recoverable with more than 99.3% accuracy. It is observed that the maximum RMSE and the voltage error values for the estimated voltages are 0.660% and 0.288%, respectively. Fig. 13 shows the corrupted ($\hat{v}$), recovered (v), and the ground-truth ($\tilde{v}$) voltage values for selected buses. Maximum percentage error for estimated statuses of lines is less than 10^{-6}, leading to a very good pursuit of ground-truth values as shown in Fig. 14. It should be observed here that, in the case of a line removal, $x_l = 0$ for every $l = (a, b) \in \mathcal{L}$, the direct voltage correlation between buses a and b disappears. The internal droop mechanism of power converters regulates their output voltage such that physical laws, presented in (1)-(2) and (14a)-(14b), are conserved independent of the line status. Fig. 15 highlights the variations on ground-truth voltage levels at bus 4, which has the highest connectivity with neighboring buses, due to changes in topology and load power trajectories. The determination of the states and topology configurations in the presence of measurement gross errors takes 4.645 s on average.

V. Conclusion

This paper offers a convex optimization framework to solve the state estimation and topology identification problems using only a limited number of measurement for converter-augmented DC networks. This problem is formulated as a constrained minimization problem, where a proper choice of objective function obviates any tuning coefficient in the absence of measurement noise. The problem formulation is then extended for the noisy measurements by adding auxiliary variables to account for convex regularization terms in the objective function. The proposed method is studied where the set of measurements are: (i) voltage values at some of the randomly-chosen buses, (ii) current-injection values at some of the randomly-chosen buses, and (iii) some of the line statuses. The convex formulation in the absence of measurement noise is validated through numerical tests using IEEE 9-bus, 14-bus, and 30-bus benchmarks, and HIL experimentation using modified IEEE 14-bus system. Furthermore, the solution in the presence of 1% measurement noise is verified through HIL experimentation on the IEEE 14-bus

system. With the help of an additional set of measurements, this solution can handle scenarios where each measurement is corrupted either by zero-mean Gaussian noises with 1% standard deviation or 100% of the corresponding original values.

APPENDIX

This section presents model matrices and vectors from network characteristics using the example of 3-bus network in Fig. 1. The bus conductance matrix of 3-bus network is calculated as

$$\boldsymbol{G} = \begin{bmatrix} g_{12}+g_{13} & -g_{12} & -g_{13} \\ -g_{21} & g_{21}+g_{23} & -g_{23} \\ -g_{31} & -g_{32} & g_{31}+g_{32} \end{bmatrix}. \tag{A.1}$$

The line conductance matrices, *from* and *to*, can be formed as

$$\vec{\boldsymbol{G}} = \begin{bmatrix} g_{12} & -g_{12} & 0 \\ g_{13} & 0 & -g_{13} \\ 0 & g_{23} & -g_{23} \end{bmatrix}, \quad \overleftarrow{\boldsymbol{G}} = \begin{bmatrix} -g_{12} & g_{12} & 0 \\ -g_{13} & 0 & g_{13} \\ 0 & -g_{23} & g_{23} \end{bmatrix}. \tag{A.2}$$

The network *from* and *to* bus-line incidence matrices for 3-bus network are

$$\vec{\boldsymbol{L}} = \begin{bmatrix} 1 & 0 & 0 \\ 1 & 0 & 0 \\ 0 & 1 & 0 \end{bmatrix}, \quad \overleftarrow{\boldsymbol{L}} = \begin{bmatrix} 0 & 1 & 0 \\ 0 & 0 & 1 \\ 0 & 0 & 1 \end{bmatrix}. \tag{A.3}$$

It can be observed that $\boldsymbol{G}$ can be derived from $(\vec{\boldsymbol{G}}^{\top}\,\vec{\boldsymbol{L}} + \overleftarrow{\boldsymbol{G}}^{\top}\,\overleftarrow{\boldsymbol{L}})$ that is also chosen as the basis matrix $\boldsymbol{M}$. The basis matrix $\boldsymbol{N}$, that is designed to penalize power loss over all the lines, is formed as

$$\boldsymbol{N} = \begin{bmatrix} 1 & 0 & 0 \\ 0 & 1 & 0 \\ 0 & 0 & 1 \end{bmatrix}. \tag{A.4}$$

The vectors of voltages, currents, and statuses of lines can be formed based on the sensors positioning shown in Fig. 1

$$\boldsymbol{v} = \begin{bmatrix} \hat{v}_1 \\ v_2 \\ v_3 \end{bmatrix}, \quad \boldsymbol{x} = \begin{bmatrix} x_1 \\ \hat{x}_2 \\ x_3 \end{bmatrix}, \quad \boldsymbol{i} = \begin{bmatrix} \hat{\imath}_1 \\ \hat{\imath}_2 \\ i_3 \end{bmatrix}. \tag{A.5}$$

Herein, measured values are utilized to infer unknown voltages v_2, v_3, and statuses of the unmonitored lines, x_1, x_3. It should be noted that the bus 3 is a zero-injection bus, and it can facilitate the performance of (4) by using $i_3 = 0$ as an additional constraint.

Finally, the auxiliary variable matrix $\boldsymbol{A}$, accounting for $\boldsymbol{v}\boldsymbol{x}^{\top}$, takes the following form

$$\boldsymbol{A} = \begin{bmatrix} \hat{v}_1 x_1 & \hat{v}_1 \hat{x}_2 & \hat{v}_1 x_3 \\ v_2 x_1 & v_2 \hat{x}_2 & v_2 x_3 \\ v_3 x_1 & v_3 \hat{x}_2 & v_3 x_3 \end{bmatrix}. \tag{A.6}$$

ACKNOWLEDGMENT

The authors are thankful to dSPACE Inc. and Typhoon HIL Inc. for allowing us to use the images of their products.

REFERENCES

[1] A. Monticelli, "Electric power system state estimation," *Proc. IEEE*, vol. 88, no. 2, pp. 262–282, Feb. 2000.
[2] E. Caro, A. J. Conejo, and A. Abur, "Breaker status identification," *IEEE Trans. Power Syst.*, vol. 25, no. 2, pp. 694–702, May 2010.
[3] G. N. Korres and P. J. Katsikas, "Identification of circuit breaker statuses in WLS state estimator," *IEEE Trans. Power Syst.*, vol. 17, no. 3, pp. 818–825, Aug. 2002.
[4] O. Alsac, N. Vempati, B. Stott, and A. Monticelli, "Generalized state estimation," *IEEE Trans. Power Syst.*, vol. 13, no. 3, pp. 1069–1075, Aug. 1998.
[5] V. Kekatos and G. B. Giannakis, "Joint power system state estimation and breaker status identification," in *Proc. North Amer. Power Symp.*, Sep. 2012, pp. 1–6.
[6] A. Monticelli, *State Estimation in Electric Power Systems: A Generalized Approach*. Berlin, Germany: Springer, 2012.
[7] G. Wang, H. Zhu, G. B. Giannakis, and J. Sun, "Robust power system state estimation from rank-one measurements," *IEEE Trans. Control Netw. Syst.*, vol. 6, no. 4, pp. 1391–1403, Dec. 2019.
[8] Y. Lin and A. Abur, "Robust state estimation against measurement and network parameter errors," *IEEE Trans. Power Syst.*, vol. 33, no. 5, pp. 4751–4759, Sep. 2018.
[9] G. He, S. Dong, J. Qi, and Y. Wang, "Robust state estimator based on maximum normal measurement rate," *IEEE Trans. Power Syst.*, vol. 26, no. 4, pp. 2058–2065, Nov. 2011.
[10] V. Kekatos and G. B. Giannakis, "Distributed robust power system state estimation," *IEEE Trans. Power Syst.*, vol. 28, no. 2, pp. 1617–1626, May 2013.
[11] M. Göl and A. Abur, "LAV based robust state estimation for systems measured by PMUS," *IEEE Trans. Smart Grid*, vol. 5, no. 4, pp. 1808–1814, Jul. 2014.
[12] Y. Weng, R. Negi, C. Faloutsos, and M. D. Ilić, "Robust data-driven state estimation for smart grid," *IEEE Trans. Smart Grid*, vol. 8, no. 4, pp. 1956–1967, Jul. 2017.
[13] A. Gomez-Exposito and A. Abur, *Power System State Estimation: Theory and Implementation*. Boca Raton, FL, USA: CRC Press, 2004.
[14] H. Zhu and G. B. Giannakis, "Estimating the state of ac power systems using semidefinite programming," in *Proc. North Amer. Power Symp.*, Aug. 2011, pp. 1–7.
[15] Y. Weng, Q. Li, R. Negi, and M. Ilić, "Semidefinite programming for power system state estimation," in *Proc. IEEE Power Energy Soc. Gener. Meeting*, Jul. 2012, pp. 1–8.
[16] Y. Zhang, R. Madani, and J. Lavaei, "Conic relaxations for power system state estimation with line measurements," *IEEE Trans. Control Netw. Syst.*, vol. 5, no. 3, pp. 1193–1205, Sep. 2018.
[17] R. Madani, J. Lavaei, R. Baldick, and A. Atamtürk, "Power system state estimation and bad data detection by means of conic relaxation," in *Proc. 50th Hawaii Int. Conf. Syst. Sci.*, 2017, pp. 3102–3111.
[18] R. Madani, M. Ashraphijuo, J. Lavaei, and R. Baldick, "Power system state estimation with a limited number of measurements," in *Proc. IEEE 55th Conf. Decis. Control*, Dec. 2016, pp. 672–679.
[19] R. Madani, J. Lavaei, and R. Baldick, "Convexification of power flow equations in the presence of noisy measurements," *IEEE Trans. Autom. Control*, vol. 64, no. 8, pp. 3101–3116, Aug. 2019.
[20] Y. Yuan, O. Ardakanian, S. Low, and C. Tomlin, "On the inverse power flow problem," 2016.
[21] Y. Wu, M. Kezunovic, and T. Kostic, "Cost minimization in power system measurement placement," in *Proc. Int. Conf. Power Syst. Technol.*, Oct. 2006, pp. 1–6.
[22] A. Monticelli and F. F. Wu, "Network observability: Identification of observable islands and measurement placement," *IEEE Trans. Power App. Syst.*, vol. PAS-104, no. 5, pp. 1035–1041, May 1985.
[23] N. G. Bretas, "Network observability: Theory and algorithms based on triangular factorisation and path graph concepts," *IEEE Proc. Gener., Transmiss. Distrib.*, vol. 143, no. 1, pp. 123–128, Jan. 1996.
[24] B. Gou and A. Abur, "A direct numerical method for observability analysis," *IEEE Trans. Power Syst.*, vol. 15, no. 2, pp. 625–630, May 2000.
[25] B. Gou, "Jacobian matrix-based observability analysis for state estimation," *IEEE Trans. Power Syst.*, vol. 21, no. 1, pp. 348–356, Feb. 2006.
[26] H. R. de Oliveira Rocha, J. C. S. de Souza, and M. B. Do Coutto Filho, "Planning high quality metering systems for state estimation through a constructive heuristic," *Int. J. Elect. Power Energy Syst.*, vol. 52, pp. 34–41, 2013.

[27] Z. Wu *et al.*, "Optimal PMU placement considering load loss and relaying in distribution networks," *IEEE Access*, vol. 6, pp. 33 645–33 653, 2018.
[28] N. M. Manousakis and G. N. Korres, "An advanced measurement placement method for power system observability using semidefinite programming," *IEEE Syst. J.*, vol. 12, no. 3, pp. 2601–2609, Sep. 2018.
[29] S. Bhela, V. Kekatos, and S. Veeramachaneni, "Enhancing observability in distribution grids using smart meter data," *IEEE Trans. Smart Grid*, vol. 9, no. 6, pp. 5953–5961, Nov. 2018.
[30] K. A. Clements, "The impact of pseudo-measurements on state estimator accuracy," in *Proc. IEEE Power Energy Soc. General Meeting*, Jul. 2011, pp. 1–4.
[31] K. Dehghanpour, Z. Wang, J. Wang, Y. Yuan, and F. Bu, "A survey on state estimation techniques and challenges in smart distribution systems," *IEEE Trans. Smart Grid*, vol. 10, no. 2, pp. 2312–2322, Mar. 2019.
[32] A. J. Schmitt, A. Bernstein, and Y. Zhang, "Matrix completion for low-observability voltage estimation," 2018, *arXiv:1801.09799*.
[33] J. Comden, A. Bernstein, and Z. Liu, "Sample complexity of power system state estimation using matrix completion," 2019, *arXiv:1905.01789*.
[34] Y. Sharon, A. M. Annaswamy, A. L. Motto, and A. Chakraborty, "Topology identification in distribution network with limited measurements," in *Proc. IEEE PES Innovative Smart Grid Technol.*, Jan. 2012, pp. 1–6.
[35] L. Zhao, W. Song, L. Tong, Y. Wu, and J. Yang, "Topology identification in smart grid with limited measurements via convex optimization," in *Proc. IEEE Innovative Smart Grid Technol. - Asia*, May 2014, pp. 803–808.
[36] A. Primadianto and C. Lu, "A review on distribution system state estimation," *IEEE Trans. Power Syst.*, vol. 32, no. 5, pp. 3875–3883, Sep. 2017.
[37] J. Zhao *et al.*, "Power system dynamic state estimation: Motivations, definitions, methodologies and future work," *IEEE Trans. Power Syst.*, vol. 34, no. 4, pp. 3188–3198, Jul. 2019.
[38] G. Fiore, A. Iovine, E. De Santis, and M. D. Di Benedetto, "Secure state estimation for dc microgrids control," in *Proc. 13th IEEE Conf. Automat. Sci. Eng.*, Aug. 2017, pp. 1610–1615.
[39] W. Doorsamy and W. A. Cronje, "State estimation on stand-alone dc microgrids through distributed intelligence," in *Proc. Int. Conf. Renewable Energy Res. Appl.*, Nov. 2015, pp. 227–231.
[40] M. Angjelichinoski, Č. Stefanović, P. Popovski, A. Scaglione, and F. Blaabjerg, "Topology identification for multiple-bus dc microgrids via primary control perturbations," in *Proc. IEEE 2nd Int. Conf. DC Microgrids*, Jun. 2017, pp. 202–206.
[41] K. Gharani Khajeh, E. Bashar, A. M. Rad, and G. B. Gharehpetian, "Integrated model considering effects of zero injection buses and conventional measurements on optimal PMU placement," *IEEE Trans. Smart Grid*, vol. 8, no. 2, pp. 1006–1013, Mar. 2017.
[42] "DC in the home," 2013. [Online]. Available: https://standards.ieee.org/content/dam/ieee-standards/standards/web/governance/iccom/IC13-005-02_DC_in_the_Home.pdf
[43] "ETSI EN 300 132-3-1," 2011. [Online]. Available: https://www.etsi.org/deliver/etsi_en/300100_300199/3001320301/02.01.01_40/en_3001320301v020101o.pdf
[44] "EMerge alliance standards," 2008. [Online]. Available: http://www.emergealliance.org/Standards/OurStandards.aspx
[45] "IEC–Standardization management board–SG4 LVDC distribution systems up to 1500V DC," 2009. [Online]. Available: https://www.iec.ch/dyn/www/f?p=103:85:0::::FSP_ORG_ID,FSP_LANG_ID:6019, 25
[46] P. Nuutinen *et al.*, "Research site for low-voltage direct current distribution in a utility network–structure, functions, and operation," *IEEE Trans. Smart Grid*, vol. 5, no. 5, pp. 2574–2582, Sep. 2014.
[47] B. Marah, Y. R. Bhavanam, G. A. Taylor, M. K. Darwish, and A. O. Ekwue, "A practical application of low voltage dc distribution network within buildings," in *Proc. 52nd Int. Universities Power Eng. Conf.*, Aug. 2017, pp. 1–6.
[48] M. ApS, "The MOSEK optimization toolbox for MATLAB manual. Version 8.1." 2017. [Online]. Available: http://docs.mosek.com/8.1/toolbox/index.html
[49] M. Grant and S. Boyd, "CVX: Matlab software for disciplined convex programming, version 2.1," Mar. 2014. [Online]. Available: http://cvxr.com/cvx
[50] P. W. Sauer and M. A. Pai, *Power System Dynamics and Stability*. Englewood Cliffs, NJ, USA: Prentice–Hall, 1998, vol. 101.
[51] University of Washington, Dept. of Electrical Engineering. "Power systems test case archive," 1999. [Online]. Available: http://www.ee.washington.edu/research/pstca/
[52] O. Alsac and B. Stott, "Optimal load flow with steady-state security," *IEEE Trans. Power Appl. Syst.*, vol. PAS-93, no. 3, pp. 745–751, May 1974.

Tuncay Altun (Student Member, IEEE) received the B.Sc. and M.Sc. degrees in electrical engineering from Yıldız Technical University, Istanbul, Turkey, in 2011 and 2014, respectively. He recently received the Ph.D. degree with the University of Texas, Arlington, TX, USA. His current research interests include optimization and control for power systems applications, renewable/sustainable energy systems, microgrids, and HVDC transmission.

Ramtin Madani (Member, IEEE) received the Ph.D. degree in electrical engineering from Columbia University, New York, NY, USA, in 2015. He was a Postdoctoral Scholar with the Department of Industrial Engineering and Operations Research, University of California, Berkeley in 2016. He is an Assistant Professor with the Department of Electrical Engineering Department, University of Texas at Arlington, Arlington, TX, USA.

Ali Davoudi (Senior Member, IEEE) received the Ph.D. degree in electrical and computer engineering from the University of Illinois, Urbana-Champaign, IL, USA, in 2010. He is currently an Associate Professor with the Electrical Engineering Department, University of Texas, Arlington, TX, USA. His current research interests include various aspects of energy conversion and power electronics systems.